Energy 258 (2022) 124837

Contents lists available at ScienceDirect

Energy

journal homepage: www.elsevier.com/locate/energy

Combustion, emissions, and performance of natural gas–ammonia dual-fuel spark-ignited engine at full-load condition

Sechul Oh [a], Cheolwoong Park [a, *], Junho Oh [b], Seonyeob Kim [a], Yongrae Kim [a], Young Choi [a], Changgi Kim [a]

[a] Department of Engine Research, Environmental Systems Research Division, Korea Institute of Machinery and Materials, Republic of Korea
[b] Division of Mechanical System Engineering, Jeonbuk National University, Republic of Korea

ARTICLE INFO

Article history:
Received 7 December 2021
Received in revised form
28 June 2022
Accepted 12 July 2022
Available online 18 July 2022

Keywords:
Ammonia
Maritime engine
Natural gas
Spark-ignition engine
Nitrogen oxides
Combustion duration

ABSTRACT

In the present study, the full load performance and emission characteristics of natural gas-ammonia dual fuel engine were investigated using the experimental methodologies with three approaches. An 11–l, 6-cylinder turbocharged natural gas engine was used in the experiments and combustion parameters, such as the energy fraction of ammonia, the air-fuel ratio, and the ignition timing, were varied to assess the effect of the introduction of ammonia as a fuel. The experiments are conducted at 1100 rpm and 1000 Nm of brake toque, which is representing the maximum torque. The effect of volumetric fuel flow rate is examined in the consideration of using a certain fuel supply system. A constant flow rate of the intake air condition was evaluated under a maximum brake torque operation condition. Lastly, the thermal efficiency and exhaust gas emissions were observed with varying the air-fuel ratio at 15% of ammonia energy fraction. The experimental results showed that using the existing fuel supply system could not secure the required brake torque and the insufficient time for the complete combustion of natural gas-ammonia mixture resulted in the increase in instability and unburned fuel of combustion. Fuel NOx was dominant of NOx emissions with the introduction of ammonia.

1. Introduction

To reduce global warming, researches in transportation and power generation fields have been directed to reduce greenhouse gas (GHG) emissions, based on the concept of 'carbon neutrality'. Accordingly, strong emission standards such as EURO 7 for automobiles (EU) [1] have been ready to be implemented so that companies, research institutes, and universities have been investigating state-of-the-art technologies to prepare. Recently, strong emission standards for maritime operation (IMO 2020) [2] were also announced in April 2018 by the International Maritime Organization (IMO). According to the regulations [2], carbon intensity from ships is to be reduced by 40% by 2030, and by 70% by 2050, compared to 2008 levels. In addition, total annual greenhouse gas emissions are to be reduced by at least 50% by 2050, compared to 2008 levels. As the maritime operation lifecycle is generally much longer than the automotive lifecycle, it is generally accepted that developing technologies to meet regulations are required well before the regulations are in effect. Whereas the automotive industry has managed strict regulations (EURO 7) by increasing market share of electric vehicle and investigating e-fuel for carbon neutrality [3], the shipbuilding market cannot follow the same process due to the several reasons. First, the scale of propulsion is too large to use battery–motor systems, considering the volume and mass of battery system to be loaded [4]. In addition, fuel cell systems with compressed or liquified hydrogen fuel cannot be used because current fuel-cell technologies cannot be applied at this power scale. Second, most e-fuels such as hydrogen and methane [5] are gaseous at room temperature. Gaseous fuels are liquified before loading in a ship in large amounts, inevitably resulting in emission of boil off gas (BOG) that must be properly processed. To meet the impending regulations, biofuels [6], alcohol fuels (such as ethanol, methanol and butanol) [7] and carbon-free fuels [8] have been comprehensively investigated using a carbon capture system (CCS) during the fuel production process or exhaust gas aftertreatment, considering the well-to-wake (WTW) concept based on life cycle analysis (LCA) [9].

* Corresponding author. Department of Engine Research, Environmental Systems Research Division, Korea Institute of Machinery and Materials, Daejeon, 34103, Republic of Korea.
E-mail address: cwpark@kimm.re.kr (C. Park).

https://doi.org/10.1016/j.energy.2022.124837

Nomenclature

Abbreviation

aTDC	after top dead center
BDC	Bottom dead center
BMEP	Brake mean effective pressure
BOG	Boil off gas
CNG	Compressed natural gas
CoV	Coefficient of variation
ECU	Engine control unit
EF	Energy fraction of ammonia
GHG	Greenhouse gas
HRR	Heat release rate
InComb	Incomplete combustion loss
LHV	Lower heating value
MBT	Maximum brake torque
MFC	Mass flow controller
NOx	Nitrogen oxides
SCR	Selective catalytic reduction
TDC	Top dead center
THC	Total unburned hydrocarbon
UAV	Unmanned aerial vehicle

Acronym

atm	Atmosphere
ex	Exhaust
in	Intake

The representative carbon-free fuels are hydrogen and ammonia. Hydrogen has been mostly used in rather small-scale applications such as automotive powertrain systems [10–13] or unmanned aerial vehicle (UAV) operation [14]. It is known that hydrogen has better combustion characteristics than ammonia, including a fast laminar flame speed, a wide flammability range, a high lower heating value (LHV) per unit mass, and lower ignition energy [15]. However, liquefaction of hydrogen is difficult as a result of its extremely low boiling point (−252.9 °C at atmospheric pressure), and it produces significant BOG [16]. In addition, backfire phenomenon [12] must be resolved to ensure safe operation during whole sailing, which frequently occurs at high loads corresponding to the usual operating range of maritime engines. Considering further issues as mentioned in many previous papers such as low volumetric power density [16], maritime researchers have focused on ammonia as an alternative fuel for maritime propulsion. The advantages include easy storage at room temperature (9.90 atm at 25 °C [17]) and comparable fuel energy per unit mass of stoichiometric fuel–air mixture. The disadvantages include intrinsic toxicity and poor combustion characteristics (slow laminar flame speed and high auto-ignition temperature). To confirm the feasibility of ammonia in internal combustion engines, our previous study considered a natural gas–ammonia dual-fuel spark-ignition engine operated in low speed and low load conditions (250 Nm, 25% of maximum brake torque at 840 rpm engine speed) under which poor combustion characteristics can be properly revealed and verified [18]. With reduced carbon dioxide emissions, flammability limits were suggested in terms of the air–fuel ratio (lambda <1.5) and volume fraction of ammonia (approximately 50% due to combustion instability). In addition, the characteristics of flame propagation induced by spark-ignition were investigated using different ammonia fractions, which significantly affected the initial burn duration (ignition timing to 10% of burned mass fraction timing).

Accordingly, several recent studies have been conducted to investigate the basic characteristics of ammonia combustion. First of all, Kanoshima et al. investigated the effects of both temperature and pressure on laminar burning velocity and Markstein length of ammonia-air mixture [19]. They found that the effect of temperature for laminar flame speed of ammonia-air mixture was larger than that for methane-air mixture, expressed as the increased exponent of temperature term in laminar flame speed correlation. Second, Shi et al. studied NOx emissions from ammonia MILD combustion by conducting experiments and considering its mechanism including elementary reactions analysis [20], showing that the radical pool (e.g. O, H, and OH) can be decreased by the dilution related to the MILD combustion. Third, Niki studied the reduction in unburned ammonia and nitrous oxide (N_2O) emissions from ammonia-assisted diesel engines [21]. From this study, it was found that the pilot injection of diesel fuel can decrease both NH_3 and N_2O emissions. These studies have focused on the basic characteristics of ammonia combustion such as flame speed, NOx and NH_3 emissions so that they can be referred to succeed our previous work as mentioned earlier. Thus, considering these studies to complete the concept of our previous research, natural gas–ammonia dual-fuel spark-ignition combustion was investigated with a full load and high engine speed (for maritime operation) as focusing on the combustion behavior (i.e. flame speed) and emissions. To extend our previous research, the following issues are addressed in this study.

1) With full-load operation, NOx emissions can be emphasized with higher temperatures (corresponding to full-load operation) of burned gas in the cylinder (denoted as thermal NOx). Since hydrocarbon fuel (i.e. natural gas) was used together with ammonia in this study, it is possible to compare the emissions results from the case with ammonia and natural gas 100% (denoted as 'base' condition). And the base condition has been evaluated frequently by using simulation tool in previous work [22].
2) For maritime operation, most of the propulsion process is in full-load operation; only the engine speed is controlled in detail. Thus, compared with the base condition with natural gas as the only fuel, the maximum engine output and its margin are evaluated quantitatively with different ammonia fractions.
3) As the combustion characteristics of natural gas–ammonia dual-fuel operation was fully investigated in low-load operation in our previous study, the analysis should be verified further in full-load conditions in this study to determine whether it is still valid.

The remainder of this paper is organized as follows. Section 2 presents the experimental setup, which is nearly the same as in the previous study; any changes are addressed. The experimental methodology includes three approaches: fixed volume rate of total fuel, fixed engine brake torque, and varying air–fuel ratio cases. Section 3 presents the experimental results and a detailed analysis. The conclusions are presented in Section 4.

2. Experimental setup and methodology

2.1. Experimental apparatus

The experimental setup is shown in Fig. 1. An 11−l, 6-cylinder spark-ignition engine originally fueled by compressed natural gas (CNG) was used in this study; the total displacement volume was similar to that of a single cylinder of a small maritime engine. Table 1 shows detailed specifications of the engine, and the specifications of each device used for the measurement process are listed in Table 2. In order to fuel the engine, natural gas was supplied by using 6 injectors mounted on the intake manifold with regulated pressure (0.8 MPa). Compared to the former one (used in previous work [18]), the remarkable change was applied to the ammonia supply system as a result of the increased flow rate required for full-load operation; a commercial mass flow controller (MFC) cannot handle the flow rate. Thus, gaseous ammonia with a linear valve (A50K-M566-G10, Autonics) was used as the fuel supply system. The details of each fuel, such as LHV value and composition, are listed in Table 3. The mass flow rate of each species was measured by Coriolis mass flowmeters (CMF025 for both natural gas and ammonia) with same model since the order of flow rate for each species was similar. ECU (Doosan Infracore) and data acquisition (DAQ) system (DACOS, Dasan) connected with dynamometer (WT470, HORIBA ATS) were used to control key parameters for engine operation − engine speed, throttle position from DAQ, and spark ignition timing, injection rate of natural gas from ECU − and monitor the measured values such as exhaust temperature, air-fuel ratio, intake pressure, and engine brake torque. K-type thermocouples were used to measure the temperature of intake flow, oil, coolant and exhaust flow. The parameters related to combustion phenomenon inside the cylinder were measured and evaluated in real-time by a combustion analyzer (DWEW800, DEWETRON) with a spark plug-type pressure sensor (6118BFD35, Kistler) mounted on the #1 cylinder.

Table 1
Specifications of engine.

Type	Description
Number of cylinders	6
Bore (mm)	123
Stroke (mm)	155
Displacement volume (cc)	11,051
Compression ratio	10.5
Maximum power	222 kW/2100 rpm
Maximum torque	1150 Nm/1300 rpm

For the emissions measurement, major gaseous species such as unburned hydrocarbon (THC), methane (CH_4), carbon dioxide (CO_2), carbon monoxide, and nitrogen oxides were measured by using an emission gas analyzer system (AMA i60, AVL). Furthermore, unburned ammonia was measured by using a tunable diode laser absorption spectroscopy (TDLAS) gas analyzer (Airwell+7, KINSCO).

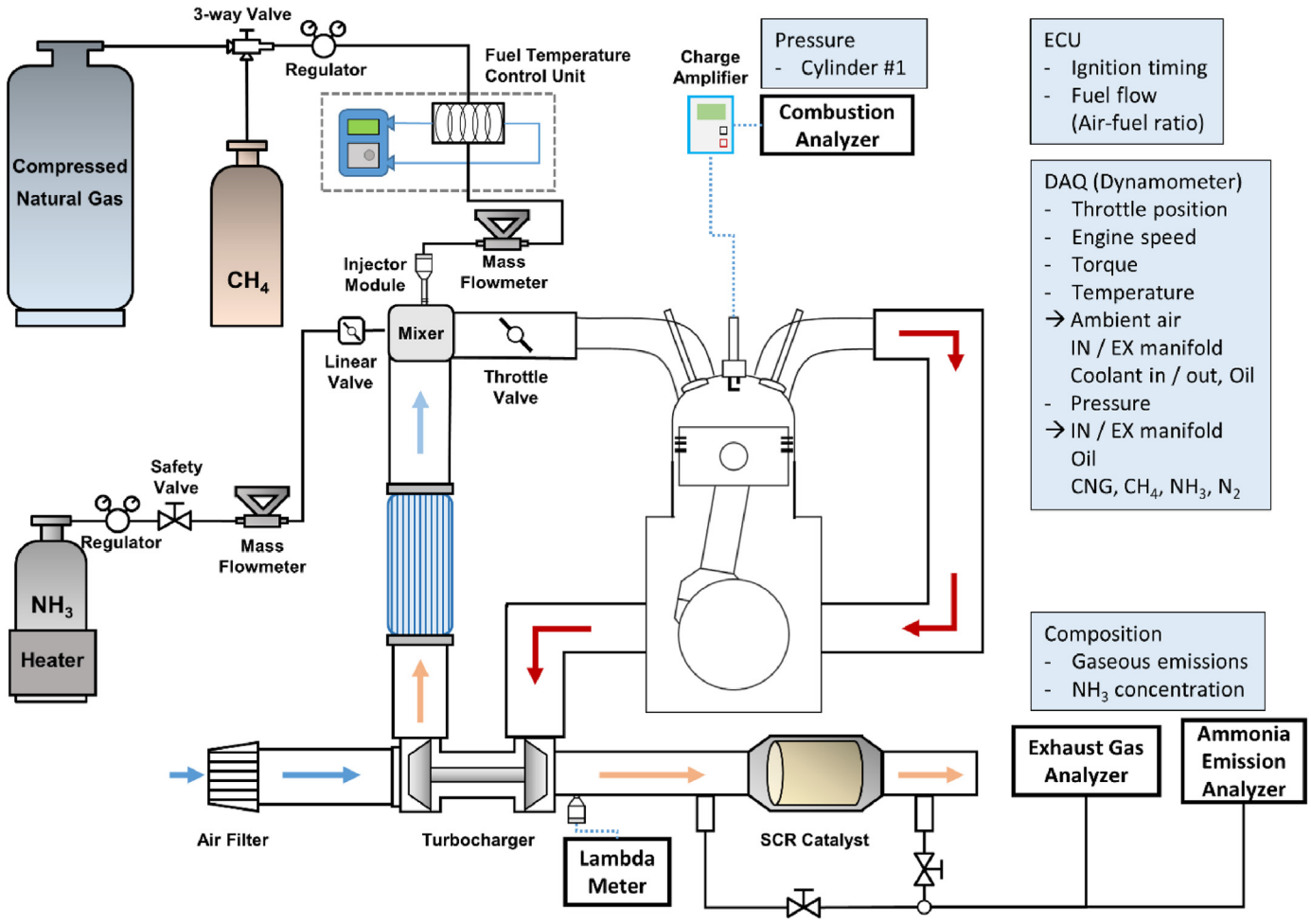

Fig. 1. Experimental configuration of dual fuel natural gas-ammonia spark ignited engine.

Table 2
Specifications of measurements.

Parameters and corresponding devices	Measuring range	Accuracy	Uncertainty
Load cell for brake torque	0-2600 Nm	0.2% of full scale	±3 Nm (about 95% confidence level, k = 2)
pressure transducer for boosted air	0–0.3 MPa (abs.)	±0.25% of full scale	±0.0004 MPa (about 95% confidence level, k = 2)
Wide band oxygen sensor for air-fuel ratio	0.125–1.25	±4.2% of full scale	±0.024 (about 95% confidence level, k = 2)
FID for THC and CH_4	0-10,000 ppm	±0.5% of full scale	±29 ppm (about 95% confidence level, k = 2)
NDIR for CO	0-10,000 ppm	±1% of full scale	±58 ppm (about 95% confidence level, k = 2)
NDIR for CO_2	0–25%	±1% of full scale	±0.29% (about 95% confidence level, k = 2)
CLD for NOx	0-10,000 ppm	±1% of full scale	±58 ppm (about 95% confidence level, k = 2)
Tunable Diode Laser Absorption Spectrometry (TDLAS) for residual ammonia	0–1000 ppm	±2% of measured value or ±2 ppm whichever is larger	±12 ppm (about 95% confidence level, k = 2)

Table 3
Characteristics of fuels used in this study.

		Natural gas (mole fraction)	Ammonia
Composition	CH_4	0.913163	0
	C_2H_6	0.054743	0
	C_3H_8	0.020618	0
	i-C_4H_{10}	0.004469	0
	n-C_4H_{10}	0.004774	0
	i-C_5H_{12}	0.000203	0
	n-C_5H_{12}	0	0
	N_2	0.002031	0
	NH_3	0	1
Lower heating value	MJ/kg	48.2	18.8
	MJ/Nm^3	38.0	14.3
Lower heating value of fuel-air mixture at stoichiometry	MJ/kg	2.76	2.64
	MJ/Nm^3	3.43	3.09
Lower heating value of fuel-air mixture at lambda = 2	MJ/kg	1.42	1.42
	MJ/Nm^3	1.80	1.73

2.2. Calculation of LHV breakdown

In this work, LHV breakdown was calculated and used for the detailed analysis of engine experiments via the terms from LHV breakdown – cooling loss, exhaust heat loss, incomplete combustion loss and gross indicated efficiency (comprising of net and pumping work). To calculate each term, GRI 3.0 mechanism [23] was used because it contains most of species of natural gas (carbon number C1, C2 and C3 – i.e. propane) and ammonia. For the calculation process, Cantera toolbox [24] was used in a MATLAB software. First of all, a composition of exhaust gas mixture is evaluated considering the atom balance of C, H, O and N between reactants and products and measured values from emission analyzer in dry condition (i.e. no H_2O). After determining exhaust gas composition, remaining LHV can be calculated so that incomplete combustion loss can be also calculated by equation (1) as listed below.

$$\text{Incomplete combustion loss} = \frac{LHV_{CO}\, n_{CO,exh} + LHV_{H_2}\, n_{H_2,exh} + LHV_{C_3H_8}\, \frac{n_{THC}-n_{CH_4}}{3} + LHV_{CH_4}\, n_{CH_4} + LHV_{NH_3}\, n_{NH_3}}{LHV_{in}} \quad \text{eq. (1)}$$

During the calculation, unburned hydrocarbon (THC) except methane was treated as propane (C_3H_8) since it had been calibrated with propane gas – 3 ppmC1 of unburned hydrocarbon is treated as 1 ppm of propane.

Second, exhaust heat loss is a portion of sensible enthalpy in exhaust gas, which is not extracted as a piston work in cylinder. It can be calculated by equation (2) as listed below [25].

$$\text{Exhaust heat loss} = \frac{\left(m_{fuel}+m_{air}\right)\left(h(T_{ex},P_{ex},x_{ex}) - h(T_{atm},P_{atm},x_{ex})\right)}{LHV_{in}} \quad \text{eq.(2)}$$

Here, the numerator represents a sensible enthalpy corresponding to the difference between exhaust and ambient temperature. After calculating these two terms and gross work (by measured in-cylinder pressure), cooling loss can be obtained by energy balance (equation (3)), which was also used for other studies [26,27].

$$\text{Cooling loss} = 1 - \text{Incomplete combustion loss} - \text{Exhaust heat loss} - \frac{\int_{BDC,\ compression}^{BDC,\ expansion} P\,dV}{LHV_{in}} \quad \text{eq. (3)}$$

2.3. Experimental methodology

To investigate full-load operation of natural gas–ammonia dual-fuel combustion, several parameters were varied, including the energy fraction of ammonia (denoted by EF, based on the LHV of ammonia and natural gas), the air–fuel ratio (presented as lambda, actual ratio over stoichiometric ratio), and the ignition timing. All experiments were conducted at 1100 rpm engine speed. Unless otherwise indicated, the maximum brake torque (MBT) with appropriate ignition timing was used, as determined in preliminary experiments. As a comparison target, the base condition was operated with 100% natural gas MBT operation. The brake torque was 1000 Nm, set as the maximum target torque (corresponding to 11.37 bar of BMEP). Lambda was 1.5, pre-determined by ECU mapping of which value is rather lean operation for NOx reduction. Considering practical issues such as sharing fuel supply systems, the experiments were conducted in three cases.

1) Case 1:The volume flow rate of natural gas in the base condition was assumed to be the maximum volume flow rate for the total fuel mixture. Under this constraint, EF was varied from 0% (base condition) to 20%, in 5% intervals with the same lambda value (1.5), based on the assumption that the same fuel supply system is used for natural gas–ammonia dual-fuel operation. As each case was conducted at MBT, the ignition timing was varied from the base case to the 20% EF case to determine the NOx emission characteristics.
2) Case 2:The brake torque was fixed at 1000 Nm for all EF conditions, the same value as the base condition. Lambda was changed by controlling the total amount of fuel with a fixed target EF. The throttle position was fixed to be the same as the base condition, assumed to be the maximum throttle valve opening corresponding to the maximum air induction. Thus, lambda was determined from the enthalpy of the exhaust mixture – the degree of turbocharging – and the total fuel rate to achieve the target brake torque. The ignition timing was varied in the same manner.
3) Case 3:As the previous experimental results were obtained with a fixed air–fuel ratio (lambda = 1.5) pre-determined for the 100% base condition (ECU mapping), it was necessary to determine whether the results and analysis were still valid for other air–fuel ratios, especially for richer conditions; the fixed lambda value (1.5) was a harsh condition for normal spark-ignition operation, as described in previous research [18] because flame initiated by spark ignition with conventional hydrocarbon fuels cannot be propagated properly at the condition of fuel-air mixture ultra-leaner (1.5 of lambda) than stoichiometry. Thus, the experiments were conducted with different air–fuel ratios, with lambda varied from 1.2 to 1.5, in intervals of 0.1 at a 15% EF. MBT operation was fixed at 1000 Nm, as in the previous experiments.

3. Experimental results and discussion

3.1. Case 1 – fixed total fuel volume flow rate

Fig. 2 shows the brake power, intake pressure, and LHV breakdown results for Case 1. It is noted that less air is required for reaction with a single mole of ammonia than with methane (main species of natural gas) at any air–fuel ratio, which can be found in the LHV of fuel-air mixture in Table 3. Thus, the throttle was closed further as the EF was increased to reduce the air flow rate for a given air–fuel ratio, as shown in Fig. 2-(a). Considering smaller LHV of ammonia than that of natural gas as shown in Table 3, total input energy per cycle was decreased by adding more ammonia with fixed volume rate of total fuel, producing a decrease in engine output from 113.7 kW in the base case to 80.5 kW in the 20% EF case, as shown in Fig. 2-(a). In Fig. 2-(b), a breakdown of LHV based on 1st law analysis is presented for each case. Although the net indicated efficiency was not consistent, it decreased in the 10% EF case, mainly due to pumping work and incomplete combustion. Here, increment in pumping work was obviously caused by closing throttle valve as mentioned. The main reason for increased incomplete combustion is, however, rather complicated to be explained. Based on the part-load results in our previous study [18], it can be inferred that due to the slow flame speed, low adiabatic

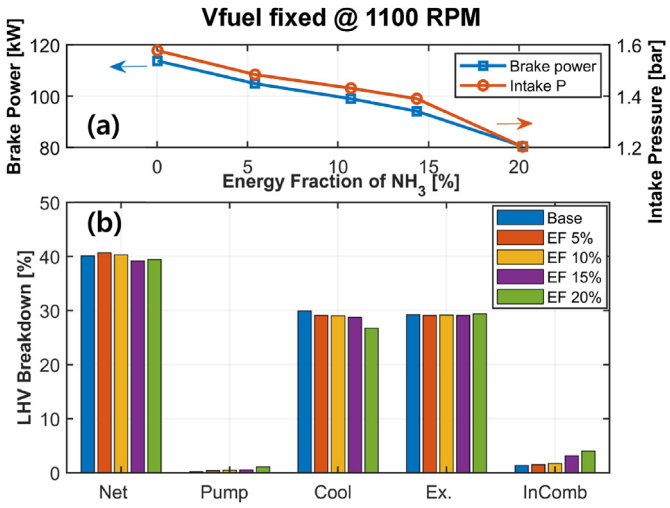

Fig. 2. Engine performance and LHV breakdown for the case 1 (fixed volume flow rate of total fuel mixture) with various EFs.

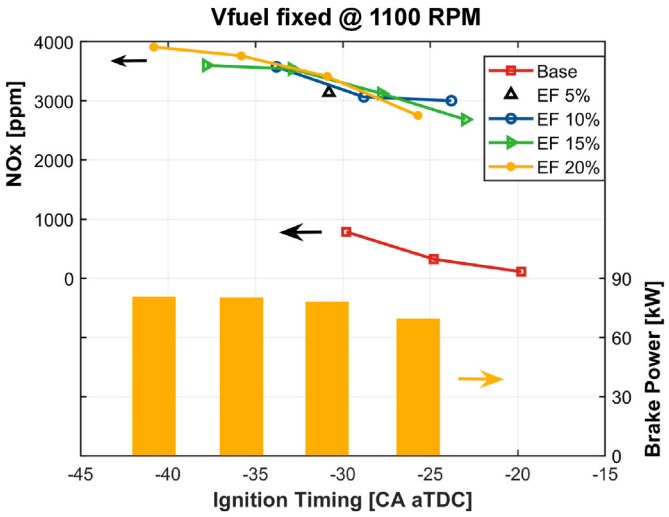

Fig. 3. NOx emissions (for all EFs) and brake power (for EF 20%) with various ignition timings (case 1).

flame temperature, and long quenching distance of ammonia [28], the flame was not fully propagated for a given engine speed, causing a monotonic increase in incomplete combustion with increasing EF. In addition, cooling loss was decreased with increasing EF, contrary to the basic trend that cooling loss is inversely proportional to engine load [29,30]. Considering the trend of adiabatic flame temperature calculated in previous research [18], a lower peak temperature in the burned zone was expected, causing a decrease in heat transfer. Quantitatively, it can be summarized as follows; until a 10% EF, net indicated efficiency showed an increasing trend with a reduction in cooling loss. After a 10% EF, increasing pumping work and incomplete combustion became main factors decreasing net indicated efficiency.

Fig. 3 shows NOx (for all EFs) and brake power (20% EF) trends with different ignition timing (x-axis). The most advanced ignition timing (leftmost) for each EF case corresponds to MBT operation, which was already analyzed. Over 2500 ppm (up to nearly 4000 ppm) of NOx emissions were produced for 5%, 10%, 15%, and 20% EF cases, mostly caused by fuel NOx produced from the flame surface, not the burned zone. The range of NOx emissions for the base condition was 111 ppm (rightmost, most retarded) to 784 ppm (leftmost, most advanced), which is in the range of thermal NOx from natural gas–air mixtures with a lambda value of 1.5. Although the total NOx emissions for each case with ammonia added cannot be clearly classified as thermal or fuel NOx, fuel NOx should be dominant in total NOx emissions considering the value with the slowest ignition timing for each case with ammonia added; little thermal NOx is expected due to delayed combustion phasing (from 2750 to 3003 ppm, greater than the range for thermal NOx).

The decrease in brake power was more significant in cases with ammonia added. Based on the present values of brake power and concentration of NOx (ppm) in Fig. 3, NOx specific emissions (expressed in g/kWh, not presented in this figure) showed similar tendency with NOx emissions denoted by [ppm] for natural gas 100% base condition – from 0.5576 (most retarded) to 3.5495 g/kWh (most advanced). For a 20% EF, however, the range of NOx emissions for a specific brake power was 16.90–18.43 g/kWh, almost unchanged due to the significant decrease in brake power, as shown in Fig. 3. To find the reason of decrease in brake power by retarding ignition timing in 20% EF, plotted in Fig. 4 were combustion-related parameters, i.e. THC, CoV (nIMEP), and ammonia emissions (denoted as a, b, and c, respectively). As the ignition timing was retarded, these variables showed a rapid increase after a certain point (e.g. −31 CA aTDC at 20% EF and −28 CA aTDC at 15% EF). In these cases, combustion was unstable (confirmed by CoV values greater than 5%), and an unburned mixture was produced, including THC, CO, CH_4, and ammonia, reducing combustion efficiency, net indicated efficiency, and brake power. As the parameters did not vary in the 100% natural gas base case, it can be inferred that the rapid change was attributed to the addition of ammonia. In other words, by increasing the fraction of ammonia of which laminar flame speed is relatively slow, the total burning speed decreased. Thus, if the ignition timing is retarded too far to allow sufficient time for a flame to propagate, such rapid increase can occur. Whether these results of fixed volume flow rate effect when introducing ammonia can be attributed to the reduction in brake power should be considered. Thus, further experiments with a fixed engine brake power are required.

3.2. Case 2 – fixed brake torque

Throughout the 2nd experiments, the brake torque was set to that of the 100% natural gas base condition, 1000 Nm at 1100 rpm. As demonstrated in the previous experiments, the total energy input per cycle decreased with increasing EF with a fixed total fuel

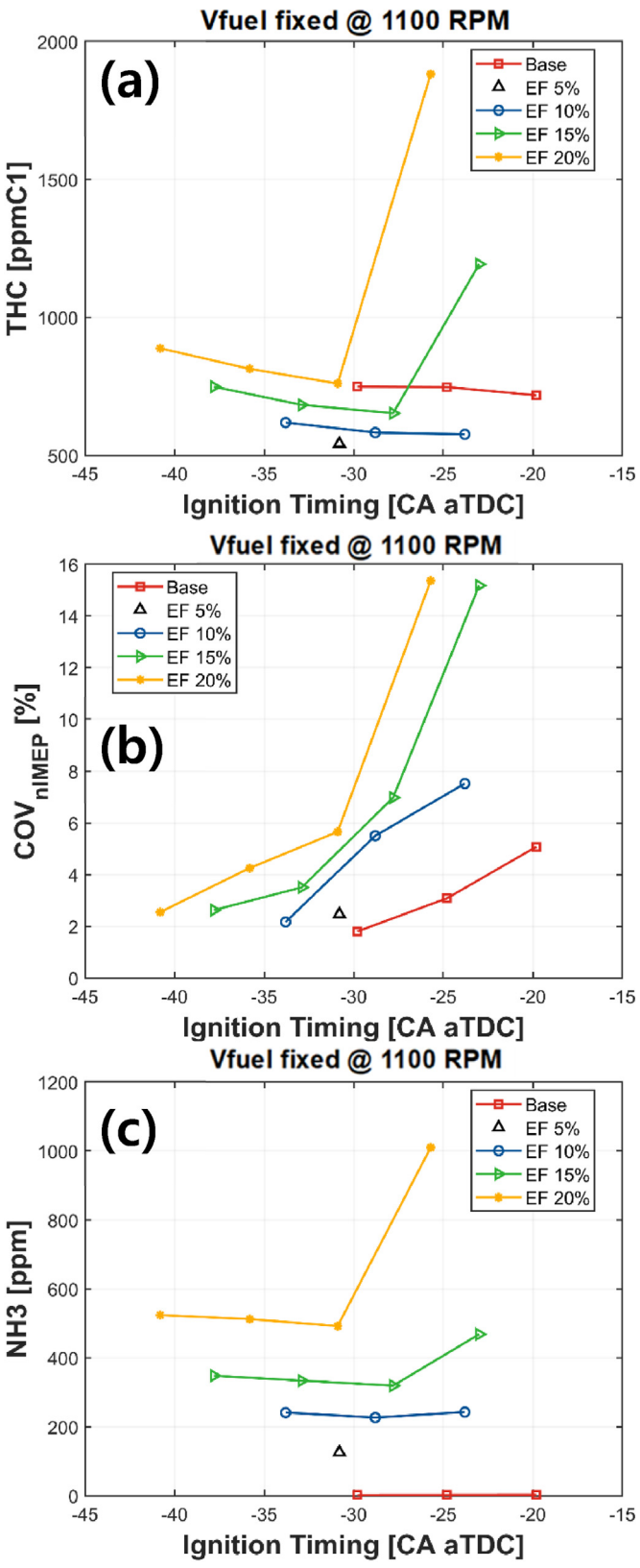

Fig. 4. THC, CoV (nIMEP), and unburned ammonia results with various ignition timings and EFs (case 1).

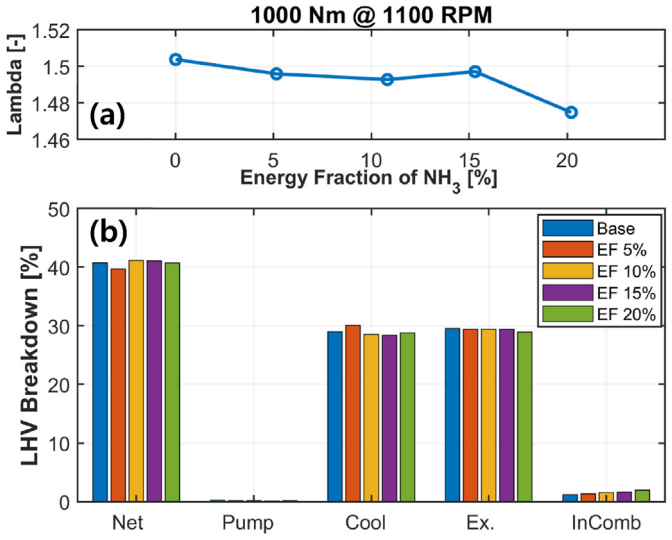

Fig. 5. Engine performance and LHV breakdown for the case 2 (fixed brake torque) with various EFs.

volume flow rate. In order to meet the same level of brake torque, the total volume flow rate must be increased for the cases with ammonia added. This can lead to a decrease in lambda – richer air–fuel ratio, depending on the net indicated efficiency for each condition. Thus, the differences in lambda (compared to 1.5 for the base condition) and net indicated efficiency should be considered together, as shown in Fig. 5. The results show that lambda decreased to 1.475 at a 20% EF, which is a minor difference considering the negative effects of ammonia on brake torque including a slow flame speed and significant incomplete combustion. Thus, it can be concluded that there is a margin to add more fuel to increase brake power, at least up to a 20% EF.

As verified in the LHV breakdown results shown at the Fig. 5-b, the net indicated efficiency showed almost no change except in the 5% case. The pumping work was negligible due to the WOT operation; the exhaust heat loss exhibited a similar trend in all cases except for 20% EF. The combustion efficiency steadily decreased as EF increased, similar to previous experiments despite the same brake power.

The combustion instability (CoV (nIMEP)) and exhaust characteristics (NOx, THC, and ammonia) were reconsidered with different ignition timings and fixed brake power constraint. To

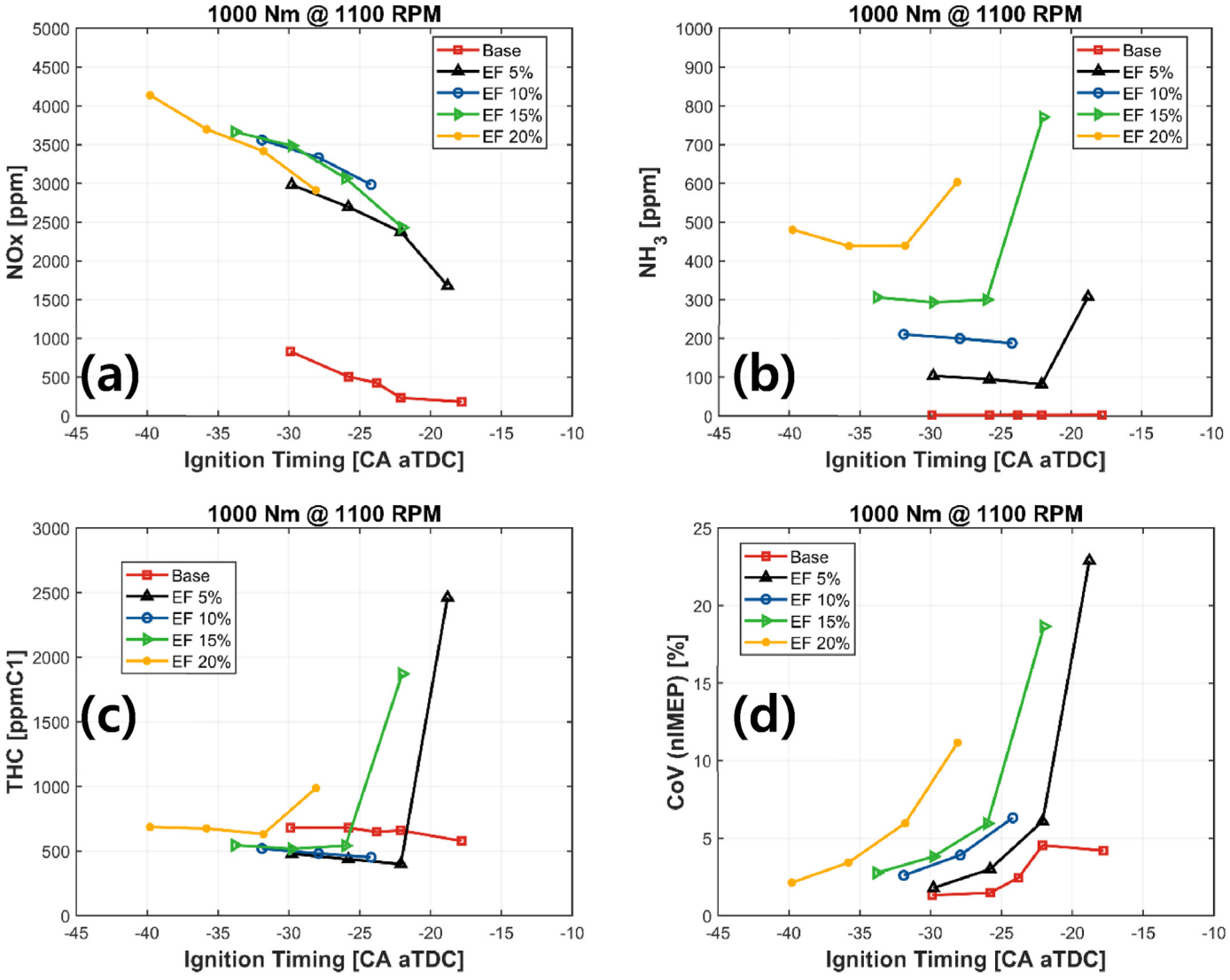

Fig. 6. NOx, unburned ammonia, THC, and CoV (nIMEP) with various ignition timings and EFs (case 2).

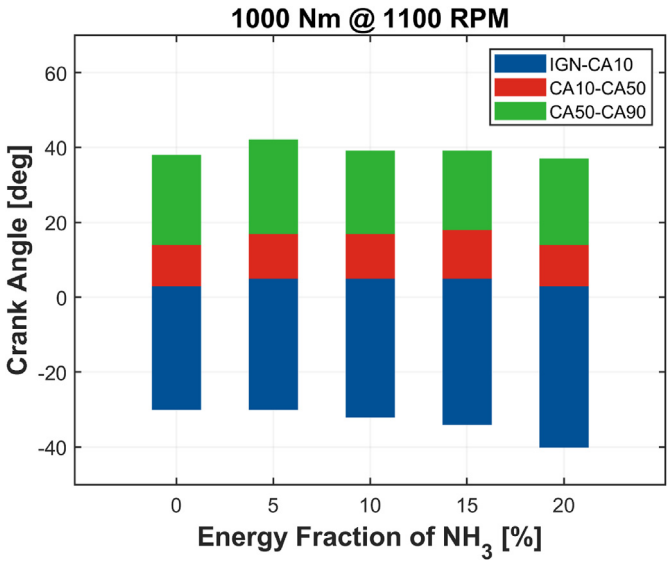

Fig. 7. Combustion phasing with various EFs (case 2).

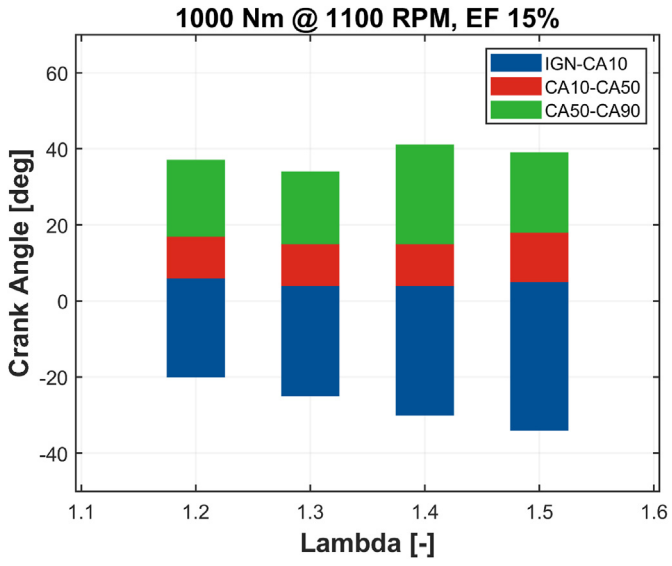

Fig. 9. Combustion phasing with various air-fuel ratios (case 3).

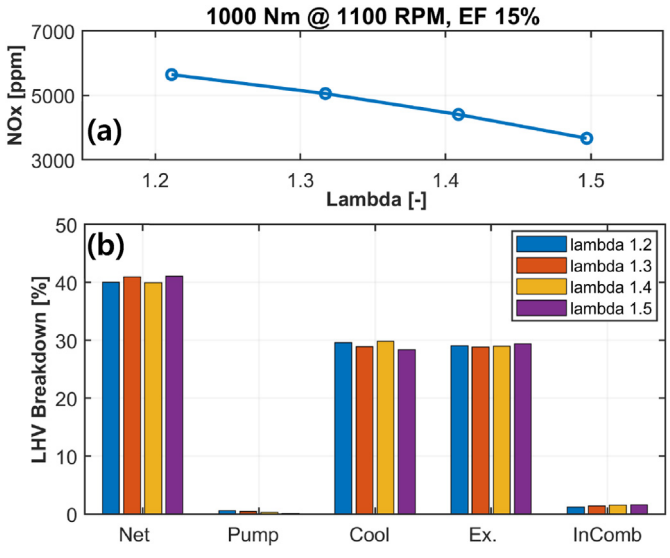

Fig. 8. NOx emissions and LHV breakdown for the case 3 with various air-fuel ratios (denoted by lambda).

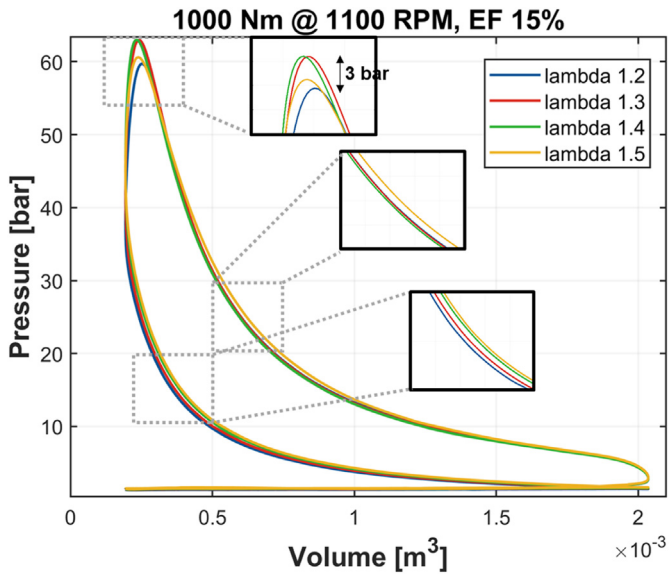

Fig. 10. In-cylinder pressure-volume profile with various air-fuel ratios (case 3).

ensure the reproducibility and consistency of the experiments, the base condition was repeated on the same day as the other experiments with ammonia added. All cases with ammonia added were conducted with a higher engine load than in the earlier experiments so that NOx emissions for each MBT operation (leftmost) were slightly higher, as shown in Fig. 6-a. The range of NOx emissions with different ignition timings, however, was almost the same. Comparing the NO_x emission results of the base condition using 100% natural gas fuel in this study with the condition in which part of natural gas is replaced to ammonia, since there is no nitrogen atom in the fuel for the base condition, the nitrogen oxide generating mechanism is dominant in thermal NO_x, and the level is less than 1000 ppm. However, when once ammonia is introduced and combustion occurs, the emission of NOx increases significantly compared to the base condition based on the MBT ignition timing. As the ignition timing advances, the trend and the extent of the increase in NO_x are at a similar level. As a result, as the energy fraction of ammonia increases, the fuel NO_x emission by nitrogen atoms in the fuel increases linearly, which has an effect on NO_x emission. The increase in NO_x emission according to the advance of ignition timing is a result of showing the thermal NO_x emission trend at a level similar to that of the base condition.

For residual ammonia at full load as shown in Fig. 6-b, the experimental results for low-load operation described in our previous study should be considered. As shown in Fig. 12 in the previous paper [18], the LHV proportion of unburned ammonia in the exhaust gas increased as the ignition timing was advanced in the low-load region. This was attributed to the low temperature and pressure of the mixture at which ignition occurred, causing unstable initial development of flame and, eventually, unstable combustion and early quenching. In the current experiments, however, the temperature and pressure were sufficiently higher than in the previous experiments (low-load); there was almost no tendency for unburned ammonia to increase with advancing

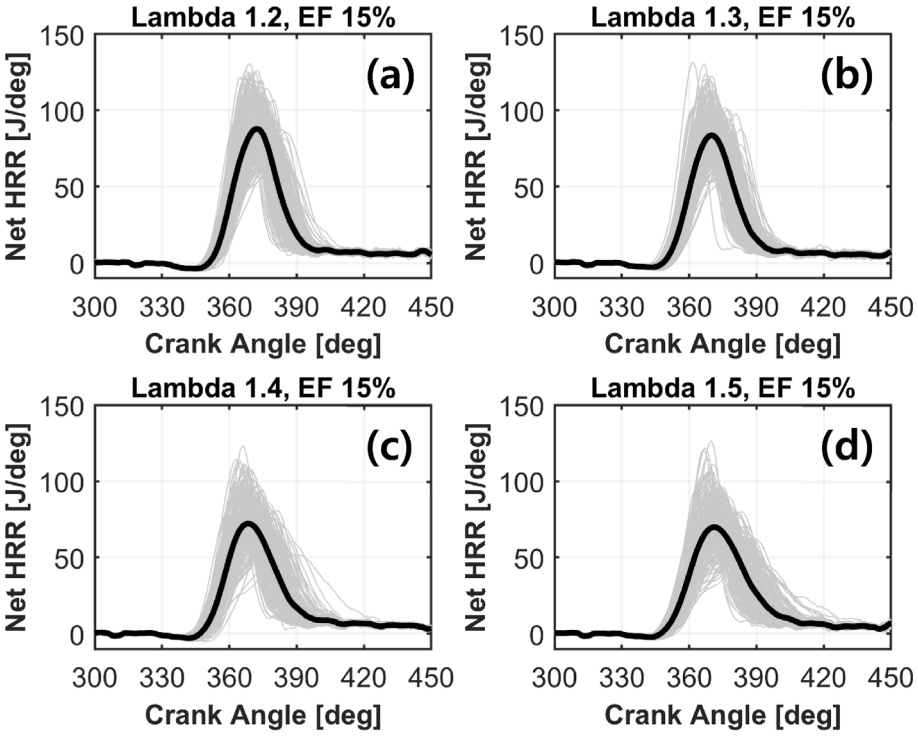

Fig. 11. Net heat release curves with various air-fuel ratio under EF 15% and 1100 RPM(black thick line: 200 cycles ensemble-averaged value, grey thin line: individual cycle, all for case 3).

ignition timing. Instead, aforementioned issue – rapid increase in CoV (nIMEP), THC and ammonia due to insufficient time for flame to be developed sufficiently – still existed despite increased brake power, as shown in Fig. 6-b, 6-c, and 6-d. Here, rapid increases in CoV (nIMEP), THC, and ammonia were produced by retarding the ignition timing (−26 CA aTDC at 15% EF). As there was no significant change in the base condition values (decreased in the most delayed case), it can be concluded that regardless of engine load, addition of ammonia can result in unstable combustion, unburned fuel (ammonia), and THC emissions, attributed to the slow flame speed of ammonia.

Considering the order of NOx and ammonia emissions, it is worth noting the possibility of using selective catalytic reduction aftertreatment system (SCR) to reduce both NOx and ammonia emissions. Clearly, urea ($CO(NH_2)_2$) would be not required thanks to the existence of ammonia in exhaust gas although its order was significantly smaller than that of NOx emissions. The amount of unburned ammonia was insufficient to reduce NOx emissions even in the slowest case with minimized NOx and maximized ammonia. Thus, additional ammonia injection into the exhaust gas may be suggested for additional NOx reduction, which is beyond our scope and considered a future work.

Fig. 7 shows the combustion phasing results obtained from the base and added ammonia cases with a fixed brake power constraint and MBT operation. Similar to the low-load experiments conducted in the previous study, ignition timing was required to be advanced with increasing EF. In addition, the initial burn duration, defined as the duration from ignition timing to 10% of the burned mass fraction timing, was also increased (slower flame propagation), which was already verified in part-load operation [18]. The main burn duration, defined as the duration from 10% to 90% of the burned mass fraction timing, did not show a clear trend; it decreased (faster flame propagation) while adding ammonia from the base to the 10% condition, then slightly increased although the difference is negligible considering calculation error during combustion phasing. Thus, it was experimentally confirmed that combustion phasing is dependent on intake composition, especially the ammonia fraction, regardless of engine load. CA50 (50% of burned mass fraction timing) was located at 14–18 CA aTDC for all conditions (MBT) due to the lean operation (lambda ~1.5); the usual stoichiometric SI engine operation with conventional fuel (gasoline) indicates 8–9 CA aTDC for CA50 with MBT operation without knock [30]. The maximum fraction of ammonia was limited to 20% due to the supply issue so that extrapolation could not be applied easily; however, the following issues are important to improve combustion characteristics of natural gas-ammonia dual fuel operation.

1) Considering that the main burn duration for a 20% EF did not decrease, only initial flame propagation with proper flame kernel development is significant for natural gas–ammonia dual-fuel operation. However, the complexity of the interaction between natural gas and ammonia during combustion is still not clear.
2) To improve the initial flame propagation from spark ignition, several methods are suggested as subjects for follow-up studies: increasing the ignition energy [31], the number of spark plugs [32], and using micropilot diesel injection as multi-point spark ignition [33]. The latest one has been actively investigated for maritime engine operation.

3.3. Case 3 – varied air–fuel ratio with fixed energy ammonia fraction

The experimental NOx emission results and LHV breakdown for Case 3 are plotted in Fig. 8-a and 8-b, respectively. Here, the NOx emissions were monotonically increased by decreasing the air–fuel

ratio. The total amount of both fuels did not change significantly as all conditions used the same brake torque. Thus, only the net indicated efficiency affected the total fuel amount; the air flow rate was controlled by throttling, such that there was a slight increase in pumping work as the air–fuel ratio was decreased. In addition, the combustion efficiency also increased, but the change in net indicated efficiency was not significant. It was governed by cooling loss; the trend was not clear.

Fig. 9 shows the combustion phasing results from the same experiments. It was found that the ignition timing, corresponding to MBT operation for each lambda, steadily decreased as the air–fuel ratio decreased, which reduced compression work. Similar to the previous study [18], initial burn duration (ignition to 10% of burned mass fraction timing) was monotonically increased (slower flame speed) with decreasing air–fuel ratio. Thus, it can be concluded that the initial burn duration was mainly affected by the air–fuel ratio and ammonia fraction rather than the load condition. The main burn duration (10% to 90% of burned mass fraction timing) increased at lambda = 1.4, then decreased with decreasing air–fuel ratio; the trend was not clear, as with the low-load operation results in previous research [18]. It can be concluded that improving the initial burn duration is important for ammonia-fueled combustion with different air–fuel ratios (not only for lambda = 1.5).

Fig. 10 shows the P–V diagram for each lambda case. The ignition timing was advanced with increasing air–fuel ratio (increased air flow rate). Thus, the in-cylinder pressure during the compression stroke increased as the air–fuel ratio increased. Near top dead center (TDC), lambda 1.3 and 1.4 cases produced high peak pressure; less fuel–air mixture reduced the peak pressure at lambda 1.2 case. The slow flame speed affected the peak pressure at lambda 1.5 case in the same manner. The maximum difference between peak pressure values was 3 bar, which was not significant. For the expansion process, lambda 1.5 case produced the highest value due to the decreased cooling loss, resulting in the maximum net indicated efficiency, as shown in Fig. 8-b. According to this, net heat release rate from individual cycles were plotted in Fig. 11. Here, ensemble-averaged value with 200 individual cycles for each case was plotted as black solid line, as HRR curves from each individual cycle for every case were plotted as thin grey line. As expected, ensemble-averaged HRR curve showed higher peak value and sharper figure in lambda 1.2, rich case. It is noted that HRR results from individual cycles for rich case (i.e. lambda 1.2) also showed sloping, narrow curve with less scattered behavior. However, as air-fuel ratio became leaner (from Figs. 11-(a) to 11-(b)), HRR curves from individual cycles showed wider, more scattered behavior, implying that burning rate became too slow to get stable combustion.

Corresponding results can be found in Fig. 12. In this figure, the unburned ammonia, THC emissions, and CoV (nIMEP) values were plotted with different air–fuel ratios. Unburned ammonia and THC emissions decreased as the air–fuel ratio was decreased (closer to stoichiometric operation). The same trend is observed in CoV values, as the difference between lambda 1.2 and 1.3 cases was negligible (0.15%). Thus, combustion characteristics can be improved by using a richer air–fuel ratio, presented as increased combustion efficiency in Fig. 8-b. However, a proper after-treatment system such as an SCR should be used to reduce NOx emissions, which exceeded 5600 ppm at lambda = 1.2, as shown in Fig. 8-a. As the air–fuel ratio decreased, NOx increased and unburned ammonia decreased, indicating that an additional reducing agent for NOx species such as urea is required to operate the SCR system properly. It is also recommended to inject additional ammonia into the exhaust mixture to prevent additional CO_2 generation from urea, although the net indicated efficiency inevitably decreases.

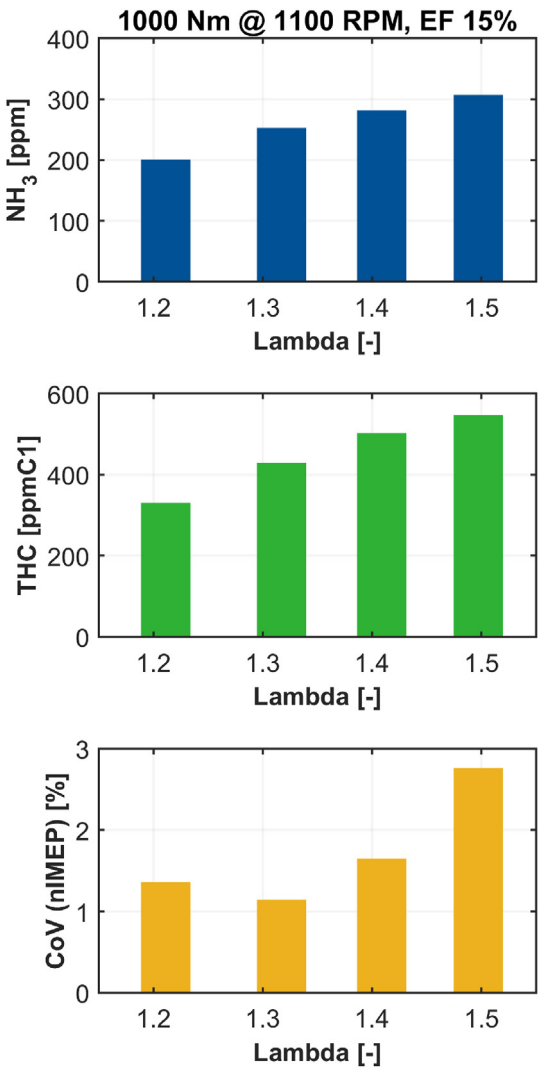

Fig. 12. Unburned ammonia, THC, and CoV (nIMEP) with various air-fuel ratios (case 3).

4. Conclusions

The experimental results of natural gas-ammonia dual fuel spark ignition engine at full-load operation were investigated in this study. New findings from this work can be summarized as follows.

1. Due to the less LHV compared to that of natural gas, ammonia addition resulted in lower brake power under same level of total volume flow rate of fuels. Despite the reduction in cooling loss with increased EF, net indicated efficiency was slightly decreased due to increased pumping and incomplete combustion loss.
2. Despite high temperature and pressure condition inside the cylinder corresponding to full-load operation, initial burn duration became longer with increased EF. It means that sufficient time should be required for proper flame propagation of ammonia-added mixture by advancing ignition timing to meet the similar level of combustion phasing (e.g. CA50); otherwise, extreme increment in incomplete combustion-related parameters – THC, CoV (nIMEP), and unburned ammonia – can occur,

regardless of the compensation of engine load by adding more fuels.

3. Fuel NOx was dominant for any cases with ammonia addition – even in the case with the smallest amount of EF (5%). It was able to be verified by the comparison between the range of thermal NOx, obtained by ignition timing variation at the base condition with 100% natural gas operation, and that of total NOx at other cases with ammonia. Total NOx emissions were monotonically increased with increasing EF and decreasing air-fuel ratio (denoted by lambda) – even over 5000 ppm of NOx emissions were measured at lambda = 1.2, EF 15% case. Despite the improvement of flame propagation speed by reducing air-fuel ratio, it should be required to adopt proper aftertreatment system to reduce NOx emissions such as SCR.

CRediT author statement

Sechul Oh: Data curation, Writing- Original draft preparation. **Cheolwoong Park:** Supervision, Methodology, Validation. **Junho Oh:** Investigation. **Seonyeob Kim:** Formal analysis. **Yongrae Kim:** Software. **Young Choi:** Resources. **Channgi Kim:** Conceptualization.

Declaration of competing interest

The authors declare that they have no known competing financial interests or personal relationships that could have appeared to influence the work reported in this paper.

Data availability

No data was used for the research described in the article.

Acknowledgement

This research was a part of the project titled 'Development of 2100 PS LNG-Ammonia dual fuel engine', funded by the Korean Ministry of Oceans and Fisheries (Project No. 1525011796) and "Development of core parts technology for non-carbon fuel main propulsion engine", funded by the Ministry of Trade, Industry and Energy, Republic of Korea (Project No. 20017612).

References

[1] European vehicle emissions standards – Euro 7 for cars, vans, lorries and buses. n.d. https://ec.europa.eu/info/law/better-regulation/have-your-say/initiatives/12313-European-vehicle-emissions-standards-Euro-7-for-cars-vans-lorries-and-buses_en. [Accessed 6 December 2021].

[2] Greenhouse gas emissions. n.d. https://www.imo.org/en/OurWork/Environment/Pages/GHG-Emissions.aspx. [Accessed 6 December 2021].

[3] Reitz RD, Ogawa H, Payri R, Fansler T, Kokjohn S, Moriyoshi Y, et al. IJER editorial: the future of the internal combustion engine. 2020.

[4] Skjong E, Volden R, Rødskar E, Molinas M, Johansen TA, Cunningham J. Past, present, and future challenges of the marine vessel's electrical power system. IEEE Trans Transp Electrif 2016;2:522–37.

[5] Kratzsch M, Wukisiewitsch W, Sens M, Brauer M, Tröger R. In: The path to CO 2-neutral mobility in 2050. Vienna Engine Symp; 2019.

[6] Mohd Noor CW, Noor MM, Mamat R. Biodiesel as alternative fuel for marine diesel engine applications: a review. Renew Sustain Energy Rev 2018;94:127–42. https://doi.org/10.1016/j.rser.2018.05.031.

[7] Rakopoulos CD, Rakopoulos DC, Kosmadakis GM, Papagiannakis RG. Experimental comparative assessment of butanol or ethanol diesel-fuel extenders impact on combustion features, cyclic irregularity, and regulated emissions balance in heavy-duty diesel engine. Energy 2019;174:1145–57.

[8] Bicer Y, Dincer I. Environmental impact categories of hydrogen and ammonia driven transoceanic maritime vehicles: a comparative evaluation. Int J Hydrogen Energy 2018;43:4583–96. https://doi.org/10.1016/j.ijhydene.2017.07.110.

[9] Singh V, Dincer I, Rosen MA. Life cycle assessment of ammonia production methods. Elsevier; 2018. https://doi.org/10.1016/B978-0-12-813734-5.00053-6.

[10] Lee J, Park C, Bae J, Kim Y, Choi Y, Lim B. Effect of different excess air ratio values and spark advance timing on combustion and emission characteristics of hydrogen-fueled spark ignition engine. Int J Hydrogen Energy 2019;44:25021–30. https://doi.org/10.1016/j.ijhydene.2019.07.181.

[11] Lee J, Park C, Kim Y, Choi Y, Bae J, Lim B. Effect of turbocharger on performance and thermal efficiency of hydrogen-fueled spark ignition engine. Int J Hydrogen Energy 2019;44:4350–60. https://doi.org/10.1016/j.ijhydene.2018.12.113.

[12] Park C, Kim Y, Choi Y, Lee J, Lim B. The effect of engine speed and cylinder-to-cylinder variations on backfire in a hydrogen-fueled internal combustion engine. Int J Hydrogen Energy 2019;44:22223–30. https://doi.org/10.1016/j.ijhydene.2019.06.058.

[13] Liu X, Srna A, Yip HL, Kook S, Chan QN, Hawkes ER. Performance and emissions of hydrogen-diesel dual direct injection (H2DDI) in a single-cylinder compression-ignition engine. Int J Hydrogen Energy 2021;46:1302–14. https://doi.org/10.1016/j.ijhydene.2020.10.006.

[14] Oh S, Park C, Nguyen D, Kim S, Kim Y, Choi Y, et al. Investigation on the operable range and idle condition of hydrogen-fueled spark ignition engine for unmanned aerial vehicle (UAV). Energy 2021;237:121645. https://doi.org/10.1016/j.energy.2021.121645.

[15] France DH. Combustion characteristics of hydrogen. Int J Hydrogen Energy 1980;5:369–74. https://doi.org/10.1016/0360-3199(80)90018-X.

[16] Van Hoecke L, Laffineur L, Campe R, Perreault P, Verbruggen SW, Lenaerts S. Challenges in the use of hydrogen for maritime applications. Energy Environ Sci 2021;14:815–43. https://doi.org/10.1039/d0ee01545h.

[17] Kobayashi H, Hayakawa A, Somarathne KDKA, Okafor EC. Science and technology of ammonia combustion. Proc Combust Inst 2019;37:109–33. https://doi.org/10.1016/j.proci.2018.09.029.

[18] Oh S, Park C, Kim S, Kim Y, Choi Y, Kim C. Natural gas–ammonia dual-fuel combustion in spark-ignited engine with various air–fuel ratios and split ratios of ammonia under part load condition. Fuel 2021;290:120095. https://doi.org/10.1016/j.fuel.2020.120095.

[19] Kanoshima R, Hayakawa A, Kudo T, Okafor EC, Colson S, Ichikawa A, et al. Effects of initial mixture temperature and pressure on laminar burning velocity and Markstein length of ammonia/air premixed laminar flames. Fuel 2022;310:122149. https://doi.org/10.1016/j.fuel.2021.122149.

[20] Shi H, Liu S, Zou C, Dai L, Li J, Xia W, et al. Experimental study and mechanism analysis of the NOx emissions in the NH3 MILD combustion by a novel burner. Fuel 2021:122417. https://doi.org/10.1016/j.fuel.2021.122417.

[21] Niki Y. Reductions in unburned ammonia and nitrous oxide emissions from an ammonia-assisted diesel engine with early timing diesel pilot injection. J Eng Gas Turbines Power 2021;143:1–7. https://doi.org/10.1115/1.4051002.

[22] Kosmadakis GM, Rakopoulos DC, Rakopoulos CD. Methane/hydrogen fueling a spark-ignition engine for studying NO, CO and HC emissions with a research CFD code. Fuel 2016;185:903–15.

[23] Smith GP, Golden DM, Frenklach M, Moriarty NW, Eiteneer B, Goldenberg M, et al. GRI 3.0 mechanism. Gas Res Inst; 1999. Http//Www Me Berkeley Edu/Gri_mech.

[24] Goodwin DG, Moffat HK, Speth RL. Cantera: an object-oriented software toolkit for chemical kinetics, thermodynamics, and transport processes. Pasadena, CA: Caltech; 2009. p. 124.

[25] Oh S. Investigation on the thermal efficiency and combustion phenomena of a direct-injected, spark-ignited engine with various conditions of stroke-to-bore ratio. 2019.

[26] Song HH. Low-load extension of residual-effected homogeneous charge compression ignition using recompression reaction. Stanford University; 2009.

[27] Splitter D, Wissink M, DelVescovo D, Reitz R. RCCI engine operation towards 60% thermal efficiency. PE, USA: SAE International Warrendale; 2013.

[28] Takizawa K, Igarashi N, Takagi S, Tokuhashi K, Kondo S. Quenching distance measurement of highly to mildly flammable compounds. Fire Saf J 2015;71:58–68. https://doi.org/10.1016/j.firesaf.2014.11.013.

[29] Heywood JB. Internal combustion engine fundamentals. McGraw-Hill Education; 2018.

[30] Oh S, Cho S, Shin W, Song C, Seol E, Min K, et al. An experimental study on the effect of stroke-to-bore ratio of Atkinson DISI engines with variable valve timing. SAE Int J Engines 2018;11:1183–94.

[31] Wei H, Zhang R, Chen L, Pan J, Wang X. Effects of high ignition energy on lean combustion characteristics of natural gas using an optical engine with a high compression ratio. Energy 2021;223:120053. https://doi.org/10.1016/j.energy.2021.120053.

[32] Gong C, Sun J, Liu F. Numerical research on combustion and emissions behaviors of a medium compression ratio direct-injection twin-spark plug synchronous ignition methanol engine under steady-state lean-burn conditions. Energy 2021;215:119193. https://doi.org/10.1016/j.energy.2020.119193.

[33] Park H, Wright YM, Seddik O, Srna A, Kyrtatos P, Boulouchos K. Phenomenological micro-pilot ignition model for medium-speed dual-fuel engines. Fuel 2021;285:118955. https://doi.org/10.1016/j.fuel.2020.118955.